

## HIGH-Z XRAY AGN CLUSTERING AND COSMOLOGICAL IMPLICATIONS

Manolis Plionis

*Institute of Astronomy & Astrophysics, National Observatory of Athens, Greece &  
 INAOE, Puebla, Mexico*



I review recent results of the high-redshift X-ray selected AGN clustering, based on the XMM/2dF survey. Using the luminosity-dependent density evolution luminosity function we find that the spatial clustering lengths, derived using Limber's inversion equation, are  $\sim 16$  and  $19 h^{-1}$  Mpc respectively (for the comoving clustering evolution model) while the median redshifts of the soft and hard X-ray sources are  $\bar{z} \sim 1.2$  and  $0.75$ , respectively. Within the framework of flat cosmological models we find that these results support a model with  $\Omega_m \simeq 0.26$ ,  $\sigma_8 \simeq 0.75$ ,  $w \simeq -0.9$  (in excellent agreement with the 3 year WMAP results). We also find the present day bias of X-ray AGNs to be  $b_o \simeq 2$ .

Active Galactic Nuclei (AGN) can be detected out to high redshifts and thus their clustering properties can provide information on the large scale structure, the underlying matter distribution and the evolution with redshift of the AGN phenomenon. From the optical 2QZ and SDSS surveys it appears that the QSO clustering properties are comparable to those of local galaxies (eg. Croom et al. 2002; 2005; Porciani, Magliocchetti & Norberg 2004; Wake et al. 2004), while there is also evidence for the comoving clustering evolution model of active galaxies (see also Kundić 1997). Optically selected AGN catalogues however, miss large numbers of dusty systems and therefore, provide a biased census of the AGN phenomenon. X-ray surveys, are least affected by dust providing an efficient tool for compiling uncensored AGN samples over a wide redshift range. From the cosmological point of view an interesting question that remains to be addressed is how the high- $z$  X-ray selected AGNs trace the underlying mass distribution and whether there are any differences with optically selected samples.

Early studies of the X-ray AGN clustering, using *Einstein* and *ROSAT* data, produced contradictory results with other studies finding significant clustering while others not (Boyle & Mo 1993; Vikhlinin & Forman 1995; Carrera et al. 1998; Akylas, Georgantopoulos & Plionis 2000; Mullis et al. 2004).

Recently, there has been an effort to address this confusing issue and determine the clustering

properties of both soft and hard X-ray selected AGNs, based on the new XMM and Chandra missions (eg. Yang et al. 2003, 2006; Basilakos et al 2004, 2005; Gilli, Daddi, Zamorani 2005; Puccetti et al. 2006; Gandhi et al. 2006). Most of these studies find a large correlation length for the high- $z$  X-ray AGNs, with hard sources having an even larger correlation length than soft sources, with  $r_o \sim 17 - 19 h^{-1}$  Mpc - (eg. Basilakos et al. 2004; Puccetti et al. 2006).

Here I review our recent results based on the 2 deg<sup>2</sup> XMM/2dF survey, which exploits the high sensitivity and the large field-of-view of the XMM-*Newton* observatory.

## 1 The XMM/2df survey: $\log N - \log S$ and $w(\theta)$

The XMM-*Newton*/2dF survey is a shallow (2-10 ksec per pointing) survey comprising of 18 XMM-*Newton* pointings equally split between a Northern and Southern Galactic region near the corresponding poles<sup>a</sup>. Due to elevated particle background we analysed a total of 13 pointings. A full description of the data reduction, source detection and flux estimation are presented in Georgakakis et al. (2003, 2004).

We will present results using the soft (0.5-2 keV), hard (2-8 keV) and total (0.5-8 keV) band catalogues of the XMM-*Newton*/2dF survey. We only consider sources at off-axis angles  $< 13.5$  arcmin. These samples comprise of 432, 171 and 462 sources respectively above the 5 $\sigma$  detection threshold. The limiting fluxes are  $f_X(0.5 - 2) = 2.7 \times 10^{-15}$  erg s<sup>-1</sup>cm<sup>-2</sup>,  $f_X(2 - 8) = 10^{-14}$  erg s<sup>-1</sup>cm<sup>-2</sup> and  $f_X(0.5 - 8) = 6.0 \times 10^{-15}$  erg s<sup>-1</sup>cm<sup>-2</sup>.

We derive the source  $\log N - \log S$  after constructing sensitivity maps in order to estimate the area of the survey accessible to point sources above a given flux limit (see Basilakos et al. 2004, 2005). In the 0.5-2 keV band there is good agreement between our results and the Baldi et al. (2002) double power-law best fit to the number counts. The Manners et al. (2003) best fit is derived for sources in the flux range  $f(0.5 - 8 \text{ keV}) = 10^{-15} - 8 \times 10^{-14}$  erg s<sup>-1</sup>cm<sup>-2</sup>. Although our  $dN/dS$  is in good agreement with their results in the above flux range, at brighter fluxes the surface density of X-ray sources is lower than the extrapolated Manners et al. (2003) relation. This suggests that a double power-law is required to fit the 0.5-8 keV  $dN/dS$  over the flux range  $10^{-15} - 10^{-12}$  erg s<sup>-1</sup>cm<sup>-2</sup>, which indeed provides an excellent fit to our  $\log N - \log S$  (see Basilakos et al. 2005).

We then calculate the angular correlation function using the estimator:  $w(\theta) = fN_{DD}/N_{DR} - 1$ , of which the uncertainty is:  $\sigma_w = \sqrt{(1 + w(\theta))/N_{DR}}$ , where  $N_{DD}$  and  $N_{DR}$  are the number of data-data and data-random pairs, respectively, in the interval  $[\theta - \Delta\theta, \theta + \Delta\theta]$ . The normalization factor is  $f = 2N_R/(N_D - 1)$ , with  $N_D$  and  $N_R$  the total number of data and random points, respectively. For each XMM pointing we produce 100 Monte Carlo random catalogues having the same number of points as the real data which also account for the sensitivity variations across the surveyed area (see section 2). Furthermore since the flux threshold for source detection depends on the off-axis angle from the center of each of the XMM-*Newton* pointing, the sensitivity maps are used to discard random points in less sensitive areas. This is accomplished by assigning a flux to each random point using the source  $\log N - \log S$ . If that flux is less than 5 times the local *rms* noise at the position of the random point (assuming Poisson statistics for the background) this is excluded from the random data-set. We have verified that our random simulations reproduce both the off-axis sensitivity of the detector as well as the individual field  $\log N - \log S$ . Using the methods described above we estimate  $w(\theta)$  in logarithmic intervals with  $\delta \log \theta \simeq 0.05$ . For all three samples we estimate  $w(\theta < 150'')$  and find a statistically significant signal (see Table 1) at a  $\gtrsim 3\sigma$  confidence level (Poisson statistics). We then use a standard  $\chi^2$  minimization procedure to fit the measured correlation function assuming a power-law form:  $w(\theta) = (\theta_o/\theta)^{\gamma-1}$  and fixing  $\gamma$  to 1.8. Note that (a) the fitting is performed for angular sepa-

---

<sup>a</sup>North: RA(J2000)=13<sup>h</sup>41<sup>m</sup>; Dec.(J2000)=00°00' ] and South: RA(J2000)=00<sup>h</sup>57<sup>m</sup>, Dec.(J2000)=-28°00'

X-ray band	No. of sources	$\theta_o$ (arcsec)	$\chi^2/\text{dof}$	$P_{\chi^2}$	$w(\theta < 150'')$
0.5-8 keV	462	$10.8 \pm 1.7$	1.50	0.10	$0.114 \pm 0.037$
0.5-2 keV	432	$10.4 \pm 1.9$	1.10	0.35	$0.105 \pm 0.035$
2-8 keV	177	$28 \pm 9$	0.88	0.57	$0.128 \pm 0.080$

Table 1: Angular correlation function analysis results with their  $1\sigma$  ( $\Delta\chi^2 = 1.00$ ) uncertainties. The fits are produced after imposing  $\gamma = 1.8$ .

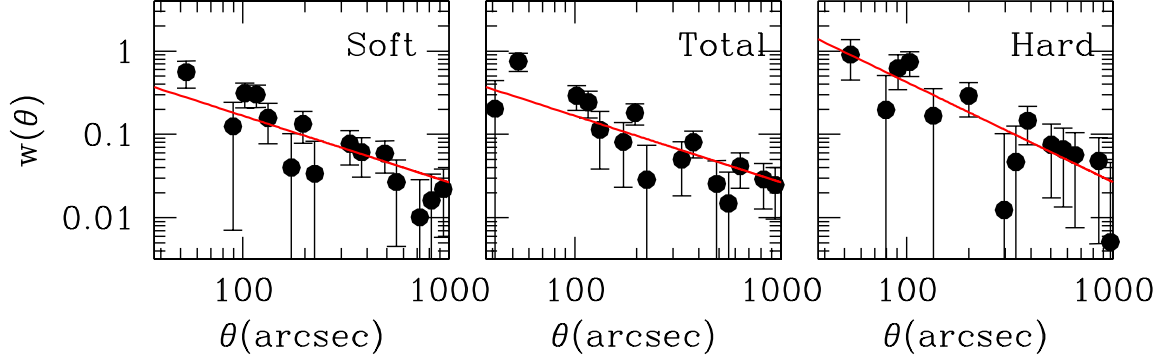


Figure 1: The XMM/2dF survey two-point angular correlation function for the 3 bands considered.

rations in the range 40–1000 arcsec, and (b) our results are insensitive to both the upper cutoff limit in  $\theta$  and the angular binning (for more than 10 bins) used to estimate  $w(\theta)$ . The resulting raw values of  $\theta_o$  are corrected for the integral constraint and the amplification bias (see Vikhlinin & Forman 1995 and Basilakos et al. 2005), although such corrections are quite small. The final results are presented in Table 1.

## 2 The spatial correlation length of the XMM/2dF soft X-ray sources

The spatial correlation function can be modeled as (eg. de Zotti et al. 1990):

$$\xi(r, z) = (r/r_o)^{-\gamma} \times (1+z)^{-(3+\epsilon)}, \quad (1)$$

where  $\epsilon$  parametrizes the type of clustering evolution. For  $\epsilon = \gamma - 3$  (ie.,  $\epsilon = -1.2$  for  $\gamma = 1.8$ ), the clustering is constant in comoving coordinates (comoving clustering), a model which appears to be appropriate for active galaxies (eg. Kundić 1997; Croom et al. 2005).

In order to invert the angular correlation function to three dimensions we utilize Limber's integral equation (eg. Peebles 1993). For a spatially flat Universe, Limber equation can be written as:

$$w(\theta) = 2 \frac{\int_0^\infty \int_0^\infty x^4 \phi^2(x) \xi(r, z) dx du}{[\int_0^\infty x^2 \phi(x) dx]^2}, \quad (2)$$

where  $\phi(x)$  is the distance selection function (the probability that a source at a distance  $x$  is detected in the survey),  $x$  is the proper distance related to the redshift through (see Peebles 1993):

$$x(z) = \frac{c}{H_o} \int_0^z \frac{dt}{E(t)} \quad \text{with} \quad E(z) = [\Omega_m(1+z)^3 + \Omega_\Lambda]^{1/2}, \quad (3)$$

The selection function,  $\phi(x)$ , is related to the number of objects in the given survey with a solid

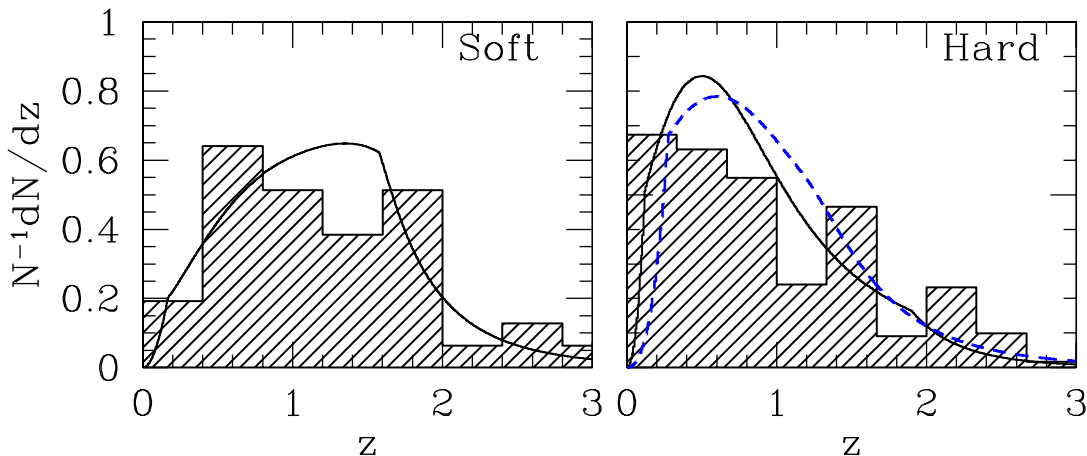


Figure 2: *Left Panel:* The expected redshift distribution (continuous line) by the Miyaji et al (2000) LDDE soft-band luminosity function. *Right Panel:* The corresponding redshift distribution for the Ueda et al. (2003) LDDE hard-band luminosity function (the dashed line is based on the La Franca et al. 2005 luminosity function). The histogram in the left panel corresponds to the distribution of the Schmidt et al (1998) X-ray sources of the ROSAT Lochman Deep Field (albeit having a flux limit slightly lower than of our survey), while that of the right panel on limited spectroscopic and photo-z data of our XMM/2dF survey.

angle  $\Omega_s$  and within the shell  $(z, z + dz)$ , by:

$$\frac{dN}{dz} = \Omega_s x^2 \phi(x) \left( \frac{c}{H_o} \right) E^{-1}(z) . \quad (4)$$

Since we do not have complete redshift information for our sources we estimate  $dN/dz$  using the X-ray source luminosity function and the specific flux-limit of our samples, via the relation:  $\phi(x) = \int_{L_{\min}(z)}^{\infty} \Phi(L_x, z) dL$ , where  $\Phi(L_x, z)$  is the luminosity dependent density evolution luminosity (LDDE) function. For the soft-band we use that of Miyaji, Hasinger & Schmidt (2000) while for the hard-band that of Ueda et al (2003). In Fig. 2 we present the expected redshift distributions of the soft and hard X-ray sources together with the histogram of some limited spectroscopic and photo-z data (see caption for details). The LDDE model predicts a redshift distribution with a median redshift of  $\bar{z} \simeq 1.2$  and  $0.75$  for the soft and hard sources respectively. Finally, the expression for  $w(\theta)$  satisfies the form:

$$w(\theta) = 2 \frac{H_o}{c} \int_0^{\infty} \left( \frac{1}{N} \frac{dN}{dz} \right)^2 E(z) dz \int_0^{\infty} \xi(r, z) du \quad (5)$$

Note that, the physical separation between two sources, separated by an angle  $\theta$  considering the small angle approximation, is given by:  $r \simeq (1+z)^{-1} (u^2 + x^2 \theta^2)^{1/2}$ .

Then the inversion of eq. (5), using the LDDE luminosity evolution model,  $\epsilon = -1.2$  and the concordance cosmological model, provides a spatial correlation length of  $r_o \simeq 16.4 \pm 1.3 h^{-1}$  Mpc and  $\simeq 19 \pm 1.3 h^{-1}$  Mpc, for the soft and hard bands, respectively. These results are in very good agreement with a recent XMM based study of the ELAIS-S1 field by Puccetti et al. (2006) and comparable to those of Extremely Red Objects (EROs), of luminous radio sources (Roche, Dunlop & Almaini 2003; Overzier et al. 2003; Röttgering et al. 2003) and of bright distant red galaxies (Foucaud et al. 2006).

Our  $r_o$  values, however, are significantly larger than those derived from optical AGN surveys (which trace mostly the unobscured component):  $r_o \simeq 5.4 - 8.6 h^{-1}$  Mpc (eg. Croom & Shanks 1996; La Franca et al. 1998; Croom et al. 2002; Grazian et al. 2004; Porciani et al. 2004; Wake et al. 2004). We can push our inverted  $r_o$  values to approximate closely the optical AGN

results only if we use the constant in physical coordinates clustering evolution model ( $\epsilon = -3$ ), in which case we obtain  $r_o \simeq 7.5 \pm 0.6 h^{-1}$  and  $\simeq 13.5 \pm 3 h^{-1}$  Mpc (for the soft and hard bands respectively).

### 3 Cosmological Constraints

It is well known (Kaiser 1984) that according to linear biasing the correlation function of the mass-tracer ( $\xi_{\text{obj}}$ ) and dark-matter one ( $\xi_{\text{DM}}$ ), are related by:

$$\xi_{\text{obj}}(r, z) = b^2(z)\xi_{\text{DM}}(r, z) , \quad (6)$$

where  $b(z)$  is the bias evolution function. In this study we use the bias model of Basilakos & Plionis 2001; 2003) which is based on linear perturbation theory and the Friedmann-Lemaitre solutions of the cosmological field equations. We quantify the underlying matter distribution clustering by presenting the spatial correlation function of the mass  $\xi_{\text{DM}}(r, z)$  as the Fourier transform of the spatial power spectrum  $P(k)$ :

$$\xi_{\text{DM}}(r, z) = \frac{(1+z)^{-(3+\epsilon)}}{2\pi^2} \int_0^\infty k^2 P(k) \frac{\sin(kr)}{kr} dk , \quad (7)$$

where  $k$  is the comoving wavenumber and  $\epsilon = -1.2$ , according to the constant in comoving coordinates clustering evolution model. As for the power spectrum, we consider that of CDM models, where  $P(k) = P_0 k^n T^2(k)$  with scale-invariant ( $n = 1$ ) primeval inflationary fluctuations. In particular, we use the transfer function parameterization as in Bardeen et al. (1986), with the corrections given approximately by Sugiyama (1995). The normalization of the power spectrum is given by:

$$P_0 = 2\pi^2 \sigma_8^2 \left[ \int_0^\infty T^2(k) k^{n+2} W^2(kR) dk \right]^{-1} . \quad (8)$$

where  $\sigma_8$  is the rms mass fluctuation on  $R = 8h^{-1}$  Mpc scales and  $W(kR)$  is the window function. Note that we also use the non-linear corrections introduced by Peacock & Dodds (1994).

We have chosen to use either the standard normalization given by:  $\sigma_8 \simeq 0.5\Omega_m^{-\gamma}$  with  $\gamma \simeq 0.21 - 0.22w + 0.33\Omega_m$  (Wang & Steinhardt 1998), or to leave  $\sigma_8$  a free parameter to be fitted by our analysis.

#### 3.1 X-ray AGN Clustering likelihood

It has been shown that the application of the correlation function analysis on samples of high redshift galaxies can be used as a useful tool for cosmological studies (eg. Matsubara 2004). In what follows we review a similar analysis, presented in Basilakos & Plionis (2005, 2006), utilizing a  $\chi^2$  likelihood procedure to compare the measured XMM soft source angular correlation function with the prediction of different spatially flat cosmological models. In particular, we define the likelihood estimator as:  $\mathcal{L}^{\text{AGN}}(\mathbf{c}) \propto \exp[-\chi_{\text{AGN}}^2(\mathbf{c})/2]$  with:

$$\chi_{\text{AGN}}^2(\mathbf{c}) = \sum_{i=1}^n \left[ \frac{w_{\text{th}}(\theta_i, \mathbf{c}) - w_{\text{obs}}(\theta_i)}{\sigma_i} \right]^2 . \quad (9)$$

where  $\mathbf{c}$  is a vector containing the cosmological parameters that we want to fit and  $\sigma_i$  the observed angular correlation function uncertainty. We assume a flat ( $\Omega_{\text{tot}} = 1$ ) cosmology with primordial adiabatic fluctuations and baryonic density of  $\Omega_b h^2 \simeq 0.022$  (eg. Kirkman et al. 2003; Spergel et al. 2006). In this case the corresponding vector is  $\mathbf{c} \equiv (\Omega_m, w, \sigma_8, h, b_o)$  and we sample the various parameters as follows: the matter density  $\Omega_m \in [0.01, 1]$  in steps of 0.01; the equation of state parameter  $w \in [-3, -0.35]$  in steps of 0.05, the power spectrum normalization

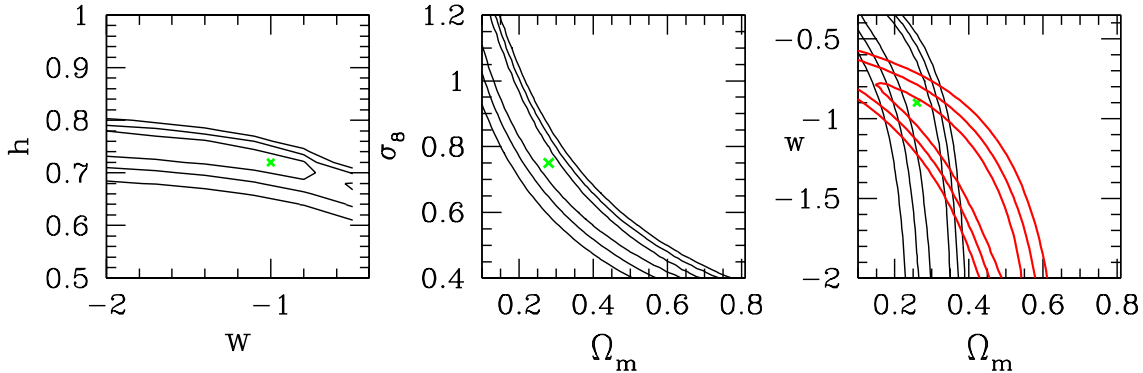


Figure 3: Likelihood contours in the  $(w, h)$  plane (left panel), the  $(\sigma_8, \Omega_m)$  plane (central panel) and the  $(w, \Omega_m)$  plane (right panel). The contours are plotted where  $-2\ln\mathcal{L}/\mathcal{L}_{\max}$  is equal to 2.30, 6.16 and 11.83, corresponding to  $1\sigma$ ,  $2\sigma$  and  $3\sigma$  confidence level. In the  $(\Omega_m, w)$  plane we plot as thick lines the likelihood contours derived from the SNIa Hubble relation.

$\sigma_8 \in [0.4, 1.4]$  in steps of 0.02, the dimensionless Hubble constant  $h \in [0.5, 0.9]$  in steps of 0.02 and the X-ray sources bias at the present time  $b_0 \in [0.5, 4]$  in steps of 0.05. Note that in order to investigate possible equations of state, we have allowed the parameter  $w$  to take values below -1. Such models correspond to the so called *phantom* cosmologies (eg. Caldwell 2002).

The resulting best fit parameters for the  $\epsilon = -1.2$  clustering evolution model are presented in Table 2. In the first two rows we present results based on the traditional Wang & Steinhardt (1998)  $\sigma_8$  normalization. Note that our estimate of the Hubble parameter  $h$  (left panel in Fig. 3) is in very good agreement with those derived ( $h = 0.72 \pm 0.07$ ) by the HST key project (Freeman et al. 2001). In the last two rows of Table 2 we leave  $\sigma_8$  free but fix the Hubble constant to  $h = 0.72$ . In Fig.3 we present the  $1\sigma$ ,  $2\sigma$  and  $3\sigma$  confidence levels in the various parameter planes, marginalizing over the rest of the parameters. We find that  $w$  is degenerate with respect to both  $h$  and the bias at the present time.

When we leave free the  $\sigma_8$  parameter, our fit (central panel of Fig. 3) provides a value which is in excellent agreement with that derived by the recent 3-years WMAP results (Spergel et al. 2006)<sup>b</sup>. Therefore, allowing for the first time values  $w < -1$  (Phantom models) we can derive a  $(\Omega_m, \sigma_8)$  relation, a good fit of which is provided by :

$$\sigma_8 = 0.34(\pm 0.01) \Omega_m^{-\gamma(\Omega_m, w)} \quad (10)$$

with  $\gamma(\Omega_m, w) = 0.22(\pm 0.04) - 0.40(\pm 0.05)w - 0.052(\pm 0.040)\Omega_m$ .

Note that eq. (10) produces  $\sigma_8$  values which are significantly smaller than the usual cluster normalization (Wang & Steinhardt 1998) but are in good agreement with the 3-years WMAP results; for example for  $w \simeq -1$  and  $\Omega_m \simeq 0.28$  we get  $\sigma_8 \simeq 0.73 \pm 0.03$ .

Inspecting the thin contours in the right panel of Fig. 3 it becomes evident that  $w$  is degenerate, within the  $1\sigma$  uncertainty, with respect to  $\Omega_m$ . Therefore, in order to put further constraints on  $w$  we additionally use a sample of 172 supernovae SNIa (see Tonry et al. 2003).

### 3.2 The AGN+SNIa likelihoods

We combine the X-ray AGN clustering properties with the SNIa data by performing a joined likelihood analysis and marginalizing the X-ray clustering results over  $\sigma_8$ ,  $h$  and  $b_0$ . The vector

<sup>b</sup>Hereafter, when we marginalize over the equation of state parameter we will use  $w = -1$ .

Data	$\Omega_m$	$\sigma_8$	$w$	$h$	$b_o$
XMM	$0.31^{+0.16}_{-0.08}$	0.93	uncons. ( $w = -1$ )	$0.72^{+0.02}_{-0.18}$	$2.30^{+0.70}_{-0.20}$
XMM/SNIa	$0.28 \pm 0.02$	0.95	$-1.05^{+0.10}_{-0.20}$	0.72	2.30
XMM	$0.28 \pm 0.03$	$0.75 \pm 0.03$	uncons. ( $w = -1$ )	0.72	$2.0^{+0.20}_{-0.25}$
XMM/SNIa	$0.26 \pm 0.04$	0.75	$-0.9^{+0.10}_{-0.05}$	0.72	2.0

Table 2: Cosmological parameters from the likelihood analysis. Errors of the fitted parameters represent  $1\sigma$  uncertainties. Note that for the joint analysis (2nd and 4th rows) the corresponding results are marginalized over the parameters that do not have errorbars, for which we use the values indicated.

$\mathbf{c}$  now becomes:  $\mathbf{c} \equiv (\Omega_m, w)$ . The SNIa likelihood function can be written as:  $\mathcal{L}^{\text{SNIa}}(\mathbf{c}) \propto \exp[-\chi_{\text{SNIa}}^2(\mathbf{c})/2]$ , with:

$$\chi_{\text{SNIa}}^2(\mathbf{c}) = \sum_{i=1}^{172} \left[ \frac{\log D_L^{\text{th}}(z_i, \mathbf{c}) - \log D_L^{\text{obs}}(z_i)}{\sigma_i} \right]^2, \quad (11)$$

where  $D_L(z)$  is the dimensionless luminosity distance,  $D_L(z) = H_o(1+z)x(z)$  and  $z_i$  is the observed redshift. The results are shown as thick lines in Fig. 3 and represent the  $1\sigma$ ,  $2\sigma$ , and  $3\sigma$ , confidence levels. The joint likelihood function ( $\mathcal{L}^{\text{joint}}(\Omega_m, w) = \mathcal{L}^{\text{AGN}} \times \mathcal{L}^{\text{SNIa}}$ ) peaks at:  $\Omega_m = 0.26 \pm 0.04$  with  $w = -0.90^{+0.1}_{-0.05}$ . Using eq. (10) we find that the normalization of the power spectrum that corresponds to these cosmological parameters is  $\sigma_8 \simeq 0.73$ . It should be pointed out that our results are in excellent agreement with the recent 3-year WMAP results of Spergel et al. (2006).

Other recent analyzes, utilizing different combinations of data, seem to agree with our results. For example, Sanchez et al. (2006) used the WMAP (1-year) CMB anisotropies in combination with the 2dFGRS power spectrum and found  $\Omega_m \simeq 0.24$  and  $w \simeq -0.85$ , while Wang & Mukherjee (2006) utilizing the 3-years WMAP data together with SNIa and galaxy clustering results found  $w \simeq -0.9$ .

## Acknowledgments

This presentation is based on the results of a Hellenic scientific collaboration project, entitled: 'X-ray Astrophysics with ESA's mission XMM', jointly funded by the European Union and the Greek Government in the framework of the program 'Promotion of Excellence in Technological Development and Research'. The colleagues involved in the research presented here are: Spyros Basilakos, Ioannis Georgantopoulos, Antonis Georgakakis and myself. I especially thank Spyros Basilakos for useful discussions.

## References

1. Akylas, A., Georgantopoulos, I., Plionis, M., 2000, MNRAS, 318, 1036
2. Baldi, A., Molendi, S., Comastri, A., Fiore, F., Matt, G., Vignali, C., 2002, ApJ, 564, 190
3. Bardeen, J.M., Bond, J.R., Kaiser, N. & Szalay, A.S., 1986, ApJ, 304, 15
4. Basilakos, S. & Plionis, M., 2001, ApJ, 550, 522
5. Basilakos, S. & Plionis, M., 2003, ApJ, 593, L61
6. Basilakos, S. & Plionis, M., 2005, MNRAS, 360, L35
7. Basilakos, S. & Plionis, M., 2006, ApJ, submitted ([astro-ph/0607065](#))
8. Basilakos, S., Georgakakis, A., Plionis, M., Georgantopoulos, I., 2004, ApJL, 607, L79
9. Basilakos, S., Plionis, M., Georgantopoulos, I., Georgakakis, A., 2005, MNRAS, 356, 183
10. Boyle, B. J., & Mo, H. J., 1993, MNRAS, 260, 925
11. Caldwell, R. R., 2002, Physics Letters B, 545, 23

12. Carrera, F. J., Barcons, X., Fabian, A. C., Hasinger, G., Mason, K. O., McMahon, R. G., Mittaz, J. P. D., Page, M. J., 1998, MNRAS, 299, 229
13. Croom, S. M., & Shanks, T., 1996, MNRAS, 281, 893
14. Croom, S.M., Boyle, B.J., Loaring, N.S., Miller, L., Outram, P.J., Shanks, T., Smith, R.J., 2002, MNRAS, 335, 459
15. Croom, S.M., et al., 2005, MNRAS, 365, 415
16. de Zotti, G., Persic, M., Franceschini, A., Danese, L., Palumbo, G. G. C., Boldt, E. A., Marshall, F. E., 1990, ApJ, 351, 22
17. Foucaud, S., et al., 2006, MNRAS, *submitted*, astro-ph/0606386
18. Freedman, W., L., et al., 2001, ApJ, 553, 47
19. Gandhi, P., et al., 2006, A&A *submitted*, astro-ph/0607135
20. Georgakakis, A., et al., 2004, MNRAS, 349, 135
21. Georgakakis, A., Georgantopoulos, I., Stewart, G. C., Shanks, T., Boyle, B. J., 2003, MNRAS, 344, 161
22. Gilli, R., et al. 2005, A&A, 430, 811
23. Grazian, A., Negrello, M., Moscardini, L., Cristiani, S., Haehnelt, M.G., Mataresse, S., Omizzolo, A., Vanella, E., 2004, AJ, 127, 592
24. Kaiser N., 1984, ApJ, 284, L9
25. Kirkman, D., Tytler, D., Suzuki, N., O'Meara, J.M., Lubin, D., 2003, ApJS, 149, 1
26. Kundić, T., 1997, ApJ, 482, 631
27. La Franca F., Andreani, P., Cristiani, S., 1998, ApJ, 497, 529
28. La Franca, F. et al., 2005, ApJ, 635, 864
29. Manners, J.C., et al., 2003, MNRAS, 343, 293
30. Matsubara T., 2004, ApJ, 615,573
31. Miyaji, T., Hasinger, G., Schmidt, M., 2000, A&A, 353, 25
32. Mullis C. R., Henry, J. P., Gioia I. M., Böhringer H., Briel, U. G., Voges, W., Huchra, J. P., 2004, ApJ, 617, 192
33. Overzier, R. A., Röttgering, H., Rengelink, R. B., Wilman, R. J. 2003, A&A, 405, 53
34. Peacock, A. J., & Dodds, S. J., 1994, MNRAS, 267, 1020
35. Peebles P.J.E., 1993. Principles of Physical Cosmology, Princeton University Press, Princeton New Jersey
36. Porciani, C., Magliocchetti, M. & Norberg, P., 2004, MNRAS,
37. Puccetti, S., et al., 2006, AA *submitted*, astro-ph/0607107
38. Roche, N. D., Dunlop, J., Almaini, O., 2003, MNRAS, 346, 803
39. Röttgering, H., Daddi, E., Overzier, R. A., Wilman, R. J. 2003, New Astronomy Reviews, 47, 309
40. Sanchez, A. G., Baugh, C. M., Percival, W. J., Peacock, J. A., Padilla, N. D., Cole, S., Frenk, C. S., Norberg, P., MNRAS, 366, 189
41. Spergel D. N., et al., ApJ, 2006, *submitted*, astro-ph/0603449
42. Sugiyama, N., 1995, ApJS, 100, 281
43. Tonry, et al. , 2003, ApJ, 594, 1
44. Ueda, Y., Akiyama, M., Ohta, K., Miyaji, T., 2003, ApJ, 598, 886
45. Vikhlinin, A. & Forman, W., 1995, ApJ, 455, 109
46. Wake, D.A. et al., 2004, ApJ, 610, L85
47. Wang, L. & Steinhardt, P.J., 1998, ApJ, 508, 483
48. Wang, Y. & Mukherjee, P., 2006, ApJ, *submitted*, astro-ph/0604051
49. Yang, Y., Mushotzky, R. F., Barger, A. J., Cowie, L. L., Sanders, D. B., Steffen, A. T., 2003, ApJ, 585, L85
50. Yang, Y., Mushotzky, R.F., Barger, A.J., Cowie, L.L., 2006, ApJ, 645, 68